ACADEMIC PRESS

Available online at www.sciencedirect.com

SCIENCE DIRECT®

Journal of Sound and Vibration 269 (2004) 549–567

JOURNAL OF SOUND AND VIBRATION

www.elsevier.com/locate/jsvi

Effect of ACLD treatment configuration on damping performance of a flexible beam

L.C. Hau, E.H.K. Fung*

Department of Mechanical Engineering, The Hong Kong Polytechnic University, Hung Hom, Kowloon, Hong Kong People's Republic of China

Received 28 May 2002; accepted 9 January 2003

Abstract

A clamped–free beam with partial active constrained layer damping (ACLD) treatment is modelled by using the finite element method. The Golla–Hughes–McTavish (GEM) method is employed to account for the frequency-dependent characteristic of the viscoelastic material (VEM). As the resultant finite element model contains too many degrees of freedom due to the introduction of dissipative coordinates, a model reduction is performed to bring the system back to its original size. Finally, optimal output feedback gains are designed based on the reduced models. Numerical simulations are performed to study the effect of different ACLD treatment configurations, with various element numbers, spacing and locations, on the damping performance of a flexible beam. Results are presented for damping ratios of the first two vibration modes. It is found that to enhance the second mode damping, without deteriorating the first mode damping, splitting a single ACLD element into two and placing them at appropriate positions of the beam could be a possible solution.

1. Introduction

Traditionally, passive constrained layer damping (PCLD) treatments are employed to damp out the vibrations of structures due to their reliability and simplicity, but the drawback of them is that once installed, the damping cannot be adjusted, and they fail to adapt to the changing environment. In other words, they are not "smart". Recently, active damping has received much attention, yet it is difficult to implement at high-frequency ranges. Safety and reliability cannot be guaranteed as well. The respective loopholes of the passive and active damping lead to the

*Corresponding author. Tel.: +852-2766-6647; fax: +852-2365-4703.
E-mail address: mmhkfung@polyu.edu.hk (E.H.K. Fung).

0022-460X/03/$ - see front matter
doi:10.1016/S0022-460X(03)00041-5

development of the so-called hybrid damping. Active constrained layer damping (ACLD) treatments, in which a piezoelectric (PZT) layer is used to replace the constraining layer of PCLD treatment, thereby integrating the advantages of both passive and active damping, has been proposed. As a result, a smart, fail-safe and efficient vibration control over broad frequency bands can be obtained.

However, it is well known that the performance of ACLD treatment highly depends on the combinations of design variables. Some parametric studies have been conducted by several researchers. Huang et al. [1] studied the performance of a hybrid-damped beam with different sizing, length, and thickness of treatments. The structure considered is partially covered by one ACLD element only and just a simple velocity feedback control is used. Trindade et al. [2] analyzed and compared the performance of segmented hybrid damping of a cantilever beam with that of a passive one for various viscoelastic layer thickness and treatment length. Baz and Ro [3] developed optimal design and control strategies for a beam fully treated with ACLD elements. The design parameters include the thickness and shear modulus of the viscoelastic layer and the control gains. Liao and Wang [4] investigated the viscoelastic material (VEM) effect on active constrained-layer-based structures. They focused on how the VEM parameter will influence the passive damping ability, the active action authority and their combined effect in ACLD configuration.

This work aims at studying the effect of different ACLD treatment configurations on the system damping of a flexible beam. A clamped–free beam with partial ACLD treatment is modelled by using the finite element method. The Golla–Hughes–McTavish (GHM) method is employed to account for the frequency-dependent characteristic of the VEM. As the resultant finite element model contains too many degrees of freedom (d.o.f) due to the addition of dissipative co-ordinates, a model reduction is performed to bring the system back to its original size. Optimal output feedback gains are then designed based on the reduced models. Finally, simulation results are presented for the damping ratios of the first two modes of vibration.

2. Finite element model

Figs. 1a and b show a clamped–free beam with one and two ACLD elements, respectively. A finite element model is developed based on the following assumptions:

(1) The rotary inertia is negligible. Shear deformations in the PZT layers and the base beam are negligible.
(2) The transverse displacement w is the same in all layers.
(3) Young's modulus of the VEM is negligible compared to those of the beam and PZT materials.
(4) Linear theories of elasticity, viscoelasticity and piezoelectricity are used.
(5) There is perfect continuity at the interface, and no slip occurs between the layers.
(6) The applied voltage is uniform throughout the ACLD element.

The model for the clamped–free beam with partial ACLD treatments is divided into treated beam elements and pure beam elements.

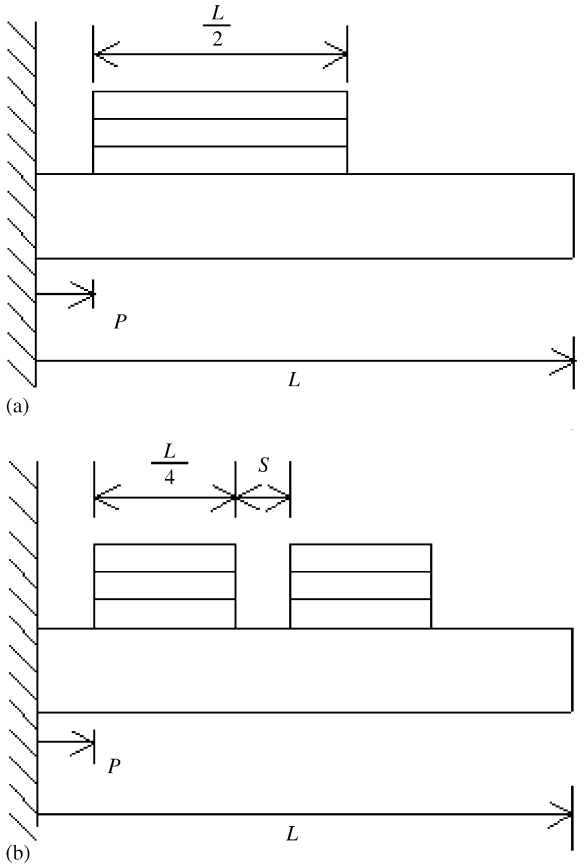

Fig. 1. (a). Clamped–free beam partially treated with one ACLD element—Case I. (b) Clamped–free beam partially treated with two ACLD elements— Case II.

2.1. Treated beam elements

2.1.1. Kinematics relationships

The geometry and deformation of the section of the beam where ACLD element is attached is shown in Fig. 2. The axial displacement of the neutral axis of the base beam, the sensor layer, the VEM layer and the constraining layer are u_b, u_s, u_v and u_c, respectively. w and θ denote the transverse displacement and rotation, respectively. The shear strain of the VEM layer is given by

$$\gamma = \theta - \psi, \tag{1}$$

where ψ is the shear angle of the VEM layer. With perfect bonding conditions, the following kinematics relations could be derived:

$$u_s = u_b - \frac{(h_c + h_b)}{2}\theta, \tag{2}$$

$$u_v = \frac{(u_b + u_c)}{2} + \frac{(h_c - 2h_s - h_b)}{4}\theta, \tag{3}$$

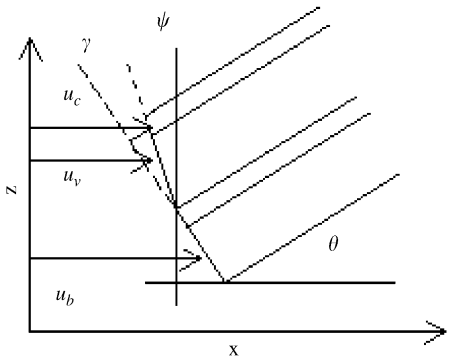

Fig. 2. Geometry and deformation of a beam with ACLD treatment.

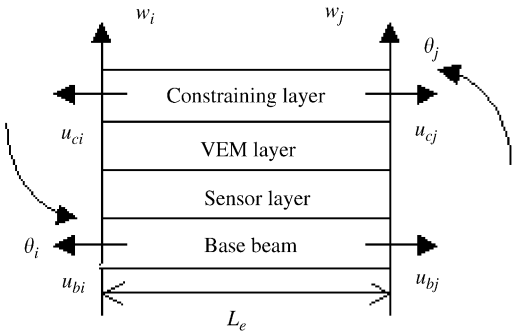

Fig. 3. Nodal displacement of a treated beam element.

$$\gamma = \frac{(u_c - u_b)}{h_v} + \frac{(h_c + 2h_v + 2h_s + h_b)}{2h_v}\theta \tag{4}$$

2.1.2. Shape functions

Fig. 3 shows a treated beam element. Nodal displacements are given by

$$\{U\}_e = \{w_i\ \theta_i\ u_{bi}\ u_{ci}\ w_j\ \theta_j\ u_{bj}\ u_{cj}\}^{\mathrm{T}}. \tag{5}$$

The transverse displacement w, the rotation θ, the axial displacement of the base beam u_b and the axial displacement of the constraining layer u_c are expressed in the nodal displacements by finite element shape functions

$$w = [N_w]\{U\}_e, \quad \theta = [N_\theta]\{U\}_e, \quad u_b = [N_{u_b}]\{U\}_e, \quad u_c = [N_{u_c}]\{U\}_e, \tag{6a–d}$$

where the shape functions are given by

$$[N_w] = \begin{bmatrix} 1-3\left(\frac{x}{L_e}\right)^2+2\left(\frac{x}{L_e}\right)^3 \\ x-2\left(\frac{x^2}{L_e}\right)+\left(\frac{x^3}{L_e^2}\right) \\ 0 \\ 0 \\ 3\left(\frac{x}{L_e}\right)^2-2\left(\frac{x}{L_e}\right)^3 \\ -\left(\frac{x^2}{L_e}\right)+\left(\frac{x^3}{L_e^2}\right) \\ 0 \\ 0 \end{bmatrix}^{\mathrm{T}}, \quad [N_\theta] = \begin{bmatrix} -6\left(\frac{x}{L_e^2}\right)+6\left(\frac{x^2}{L_e^3}\right) \\ 1-4\left(\frac{x}{L_e}\right)+3\left(\frac{x}{L_e}\right)^2 \\ 0 \\ 0 \\ 6\left(\frac{x}{L_e^2}\right)-6\left(\frac{x^2}{L_e^3}\right) \\ -2\left(\frac{x}{L_e}\right)+3\left(\frac{x}{L_e}\right)^2 \\ 0 \\ 0 \end{bmatrix}^{\mathrm{T}},$$

$$[N_{u_b}] = \left[0 \quad 0 \quad 1-\frac{x}{L_e} \quad 0 \quad 0 \quad 0 \quad \frac{x}{L_e} \quad 0\right],$$

$$[N_{u_c}] = \left[0 \quad 0 \quad 0 \quad 1-\frac{x}{L_e} \quad 0 \quad 0 \quad 0 \quad \frac{x}{L_e}\right]. \tag{6e–h}$$

From Eqs. (2)–(4), u_s, u_v and γ can be expressed in the nodal displacement as follows:

$$u_s = [N_{u_s}]\{U\}_e, \quad u_v = [N_{u_v}]\{U\}_e, \quad \gamma = [N_\gamma]\{U\}_e, \tag{7a–c}$$

where

$$[N_{u_s}] = [N_{u_b}] - \left(\frac{h_b+h_s}{2}\right)[N_\theta],$$

$$[N_{u_v}] = \frac{1}{2}([N_{u_c}]+[N_{u_b}]) + \left(\frac{h_c-2h_s-h_b}{4}\right)[N_\theta],$$

$$[N_\gamma] = \frac{1}{h_v}([N_{u_c}]-[N_{u_b}]) + \left(\frac{h_c+2h_v+2h_s+h_b}{2h_v}\right)[N_\theta]. \tag{7d–f}$$

2.1.3. Energy expressions

Base beam layer

The potential energy of base beam due to axial displacement is:

$$\frac{1}{2}\int_0^{L_e} E_b h_b b\left(\frac{\partial u_b}{\partial x}\right)^2 \mathrm{d}x = \frac{1}{2}\{U\}_e^{\mathrm{T}}[K_{bu}]\{U\}_e, \quad [K_{bu}] = E_b h_b b\int_0^{L_e}[N_{u_b}]'^{\mathrm{T}}[N_{u_b}]'\,\mathrm{d}x. \tag{8a, b}$$

The potential energy of base beam due to transverse displacement is:

$$\frac{1}{2}\int_0^{L_e} E_b I_b\left(\frac{\partial^2 w}{\partial x^2}\right)^2 \mathrm{d}x = \frac{1}{2}\{U\}_e^{\mathrm{T}}[K_{bw}]\{U\}_e, \quad [K_{bw}] = E_b I_b\int_0^{L_e}[N_w]''^{\mathrm{T}}[N_w]''\,\mathrm{d}x. \tag{9a, b}$$

The kinetic energy of base beam due to axial displacement is:

$$\frac{1}{2}\int_0^{L_e} \rho_b h_b b\left(\frac{\partial u_b}{\partial t}\right)^2 \mathrm{d}x = \frac{1}{2}\{\dot{U}\}_e^{\mathrm{T}}[M_{bu}]\{\dot{U}\}_e, \quad [M_{bu}] = \rho_b h_b b \int_0^{L_e} [N_{u_b}]^{\mathrm{T}}[N_{u_b}]\,\mathrm{d}x. \tag{10a, b}$$

The kinetic energy of base beam due to transverse displacement is:

$$\frac{1}{2}\int_0^{L_e} \rho_b h_b b\left(\frac{\partial w}{\partial t}\right)^2 \mathrm{d}x = \frac{1}{2}\{\dot{U}\}_e^{\mathrm{T}}[M_{bw}]\{\dot{U}\}_e, \quad [M_{bw}] = \rho_b h_b b \int_0^{L_e} [N_w]^{\mathrm{T}}[N_w]\,\mathrm{d}x. \tag{11a, b}$$

Constraining layer

For one-dimensional structures with uni-axial loading, the constitutive equations of PZT materials [5] can be written as

$$\begin{bmatrix} \varepsilon \\ D \end{bmatrix} = \begin{bmatrix} S_{11}^E & d_{31} \\ d_{31} & \varepsilon_{33}^{\tau} \end{bmatrix} \begin{bmatrix} \sigma \\ E \end{bmatrix}, \tag{12}$$

where D is the electrical displacement, E is the electric field, ε is the mechanical strain in the x direction, and σ is the mechanical stress in the x direction. S_{11}^E is the elastic compliance constant, ε_{33}^{τ} is the dielectric constant, and d_{31} is the piezoelectric constant.

The potential energy of constraining layer due to axial displacement is:

$$\frac{1}{2}\int_0^{L_e} E_c h_c b\left(\frac{\partial u_c}{\partial x}\right)^2 \mathrm{d}x = \frac{1}{2}\{U\}_e^{\mathrm{T}}[K_{cu}]\{U\}_e, \quad [K_{cu}] = E_c h_c b \int_0^{L_e} [N_{u_c}]'^{\mathrm{T}}[N_{u_c}]'\,\mathrm{d}x. \tag{13a, b}$$

The potential energy of constraining layer due to transverse displacement is:

$$\frac{1}{2}\int_0^{L_e} E_c I_c\left(\frac{\partial^2 w}{\partial x^2}\right)^2 \mathrm{d}x = \frac{1}{2}\{U\}_e^{\mathrm{T}}[K_{cw}]\{U\}_e, \quad [K_{cw}] = E_c I_c \int_0^{L_e} [N_w]''^{\mathrm{T}}[N_w]''\,\mathrm{d}x. \tag{14a, b}$$

The kinetic energy of constraining layer due to axial displacement is:

$$\frac{1}{2}\int_0^{L_e} \rho_c h_c b\left(\frac{\partial u_c}{\partial t}\right)^2 \mathrm{d}x = \frac{1}{2}\{\dot{U}\}_e^{\mathrm{T}}[M_{cu}]\{\dot{U}\}_e, \quad [M_{cu}] = \rho_c h_c b \int_0^{L_e} [N_{u_c}]^{\mathrm{T}}[N_{u_c}]\,\mathrm{d}x. \tag{15a, b}$$

The kinetic energy of constraining layer due to transverse displacement is:

$$\frac{1}{2}\int_0^{L_e} \rho_c h_c b\left(\frac{\partial w}{\partial t}\right)^2 \mathrm{d}x = \frac{1}{2}\{\dot{U}\}_e^{\mathrm{T}}[M_{cw}]\{\dot{U}\}_e, \quad [M_{cw}] = \rho_c h_c b \int_0^{L_e} [N_w]^{\mathrm{T}}[N_w]\,\mathrm{d}x. \tag{16a, b}$$

The virtual work done by the induced strain (force) is:

$$\delta W_c = \int_0^{L_e} E_c d_{31} b V_c(t)\delta\left(\frac{\partial u_c}{\partial x}\right)\mathrm{d}x = [\delta U]_e^{\mathrm{T}}\{f_c\}_e, \tag{17a}$$

where

$$\{f_c\}_e = E_c d_{31} b V_c(t)[0\ 0\ 0 - 1\ 0\ 0\ 0\ 1]^{\mathrm{T}}. \tag{17b}$$

Sensor layer

The potential energy of sensor layer due to axial displacement is:

$$\frac{1}{2}\int_0^{L_e} E_s h_s b\left(\frac{\partial u_s}{\partial x}\right)^2 \mathrm{d}x = \frac{1}{2}\{U\}_e^{\mathrm{T}}[K_{su}]\{U\}_e, \quad [K_{su}] = E_s h_s b \int_0^{L_e} [N_{u_s}]'^{\mathrm{T}}[N_{u_s}]'\,\mathrm{d}x. \tag{18a, b}$$

The potential energy of sensor layer due to transverse displacement is:

$$\frac{1}{2}\int_0^{L_e} E_s I_s \left(\frac{\partial^2 w}{\partial x^2}\right)^2 \mathrm{d}x = \frac{1}{2}\{U\}_e^{\mathrm{T}}[K_{sw}]\{U\}_e, \quad [K_{sw}] = E_s I_s \int_0^{L_e} [N_w]''^{\mathrm{T}}[N_w]'' \,\mathrm{d}x. \tag{19a, b}$$

The kinetic energy of sensor layer due to axial displacement is:

$$\frac{1}{2}\int_0^{L_e} \rho_s h_s b \left(\frac{\partial u_s}{\partial t}\right)^2 \mathrm{d}x = \frac{1}{2}\{\dot{U}\}_e^{\mathrm{T}}[M_{su}]\{U\}_e, \quad [M_{su}] = \rho_s h_s b \int_0^{L_e} [N_{u_s}]^{\mathrm{T}}[N_{u_s}] \,\mathrm{d}x. \tag{20a, b}$$

The kinetic energy of sensor layer due to transverse displacement is:

$$\frac{1}{2}\int_0^{L_e} \rho_s h_s b \left(\frac{\partial w}{\partial t}\right)^2 \mathrm{d}x = \frac{1}{2}\{\dot{U}\}_e^{\mathrm{T}}[M_{sw}]\{\dot{U}\}_e, \quad [M_{sw}] = \rho_s h_s b \int_0^{L_e} [N_w]^{\mathrm{T}}[N_w] \,\mathrm{d}x. \tag{21a, b}$$

VEM layer

The potential energy of VEM layer due to shear strain is:

$$\frac{1}{2}\int_0^{L_e} G_v h_v b \gamma^2 \,\mathrm{d}x = \frac{1}{2}\{U\}_e^{\mathrm{T}}[K_{v\gamma}]\{U\}_e, \quad [K_{v\gamma}] = G_v h_v b \int_0^{L_e} [N_\gamma]^{\mathrm{T}}[N_\gamma] \,\mathrm{d}x. \tag{22a, b}$$

The kinetic energy of VEM layer due to axial displacement is:

$$\frac{1}{2}\int_0^{L_e} \rho_v h_v b \left(\frac{\partial u_v}{\partial t}\right)^2 \mathrm{d}x = \frac{1}{2}\{\dot{U}\}_e^{\mathrm{T}}[M_{vu}]\{\dot{U}\}_e, \quad [M_{vu}] = \rho_v h_v b \int_0^{L_e} [N_{u_v}]^{\mathrm{T}}[N_{u_v}] \,\mathrm{d}x. \tag{23a, b}$$

The kinetic energy of VEM layer due to transverse displacement is:

$$\frac{1}{2}\int_0^{L_e} \rho_v h_v b \left(\frac{\partial w}{\partial t}\right)^2 \mathrm{d}x = \frac{1}{2}\{\dot{U}\}_e^{\mathrm{T}}[M_{vw}]\{\dot{U}\}_e, \quad [M_{vw}] = \rho_v h_v b \int_0^{L_e} [N_w]^{\mathrm{T}}[N_w] \,\mathrm{d}x. \tag{24a, b}$$

2.1.4. Sensor equation

The sensor output voltage is given by

$$\{V_s\}_e = \frac{E_s d_{31} b}{C_a}\left[0 \quad \frac{h_b}{2} + h_s \quad -1 \quad 0 \quad 0 \quad \frac{-h_b}{2} - h_s \quad 1 \quad 0\right]\{U\}_e, \tag{25}$$

where b and C_a are the width and capacitance of the sensor layer, respectively.

2.2. Pure beam elements

The stiffness and mass matrices of pure beam elements have dimensions of 6×6, and are similar to those given by Eqs. (8b), (9b), (10b) and (11b).

2.3. Load vector

The virtual work done δW_d by external disturbance force f_d is:

$$\delta W_d = \int_0^{Le} f_d(x,t)\delta w(x,t) \,\mathrm{d}x = [\delta U]_e^{\mathrm{T}}\{f_d\}. \tag{26}$$

It is usually more convenient to consider the effects of such force at the global level.

2.4. Equations of motion

Using Hamilton's principle, the equations of motion for an ACLD element can be written as

$$[M]_e\{\ddot{U}\}_e + [K]_e\{U\}_e + [K_{v\gamma}]_e\{U\}_e = \{f_c\}_e, \tag{27a}$$

where

$$[M]_e = ([M_{bu}] + [M_{bw}]) + ([M_{cu}] + [M_{cw}]) + ([M_{su}] + [M_{sw}]) + ([M_{vu}] + [M_{vw}]),$$
$$[K]_e = ([K_{bu}] + [K_{bw}]) + ([K_{cu}] + [K_{cw}]) + ([K_{su}] + [K_{sw}]). \tag{27b, c}$$

The GHM method [6,7] is now used to account for the damping due to the frequency-dependent VEM. For one-dimensional structures, the GHM model represents the shear modulus of VEM as a series of mini-oscillator terms in the Laplace domain:

$$s\tilde{G}(s) = G^{\infty}\left[1 + \sum_{k=1}^{N} \hat{\alpha}_k \frac{s^2 + 2\hat{\zeta}_k\hat{\omega}_k s}{s^2 + 2\hat{\zeta}_k\hat{\omega}_k s + \hat{\omega}_k^2}\right]. \tag{28}$$

The positive constants $\hat{\alpha}_k$, $\hat{\omega}_k$ and $\hat{\zeta}_k$ govern the shape of the modulus function over the complex s-domain. Introducing a column matrix of dissipation co-ordinates:

$$\{\hat{Z}(s)\}_e = \frac{\hat{\omega}^2}{s^2 + 2\hat{\zeta}\hat{\omega}s + \hat{\omega}^2}\{U(s)\}_e. \tag{29}$$

Considering a single-term GHM expression [4], Eq. (27) can be written as follows:

$$[\bar{M}]_e\{\ddot{q}\}_e + [\bar{D}]_e\{\dot{q}\}_e + [\bar{K}]_e\{q\}_e = \{\bar{f}_c\}_e, \tag{30a}$$

where

$$[\bar{M}]_e = \begin{bmatrix} [M]_e & [0] \\ [0] & \dfrac{\hat{\alpha}}{\hat{\omega}^2}[\Lambda] \end{bmatrix}, \quad [\bar{D}]_e = \begin{bmatrix} [0] & [0] \\ [0] & \dfrac{2\hat{\alpha}\hat{\zeta}}{\hat{\omega}}[\Lambda] \end{bmatrix},$$
$$[\bar{K}]_e = \begin{bmatrix} [K]_e + [K_{v\gamma}]_e(1+\hat{\alpha}) & -\hat{\alpha}[R] \\ -\hat{\alpha}[R]^{\mathrm{T}} & \hat{\alpha}[\Lambda] \end{bmatrix},$$
$$\{q\}_e = \begin{Bmatrix} \{U\}_e \\ \{Z\}_e \end{Bmatrix}, \quad \{\bar{f}_c\}_e = \begin{Bmatrix} \{f_c\}_e \\ \{0\} \end{Bmatrix}, \tag{30b–f}$$

where $\{Z\}_e = [\hat{R}]^{\mathrm{T}}\{\hat{Z}\}_e, [R] = [\hat{R}][\Lambda], [\Lambda] = G^{\infty}[\hat{\Lambda}], [K_{v\gamma}]_e = G^{\infty}[\hat{K}_{v\gamma}]_e, [\hat{K}_{v\gamma}]_e = [\hat{R}][\hat{\Lambda}][\hat{R}]^{\mathrm{T}}$ (30g–k)

$[\hat{\Lambda}]$ is a diagonal matrix of the non-zero (necessarily positive) eigenvalues of matrix $[\hat{K}_{v\gamma}]_e$, and the corresponding orthonormalized eigenvectors form the columns of the matrix $[\hat{R}]$.

For the clamped–free beam with distributed ACLD elements, through standard FEM assembling procedures and with appropriate boundary conditions, the following global dynamic equation can be derived:

$$[M]\{\ddot{q}\} + [D]\{\dot{q}\} + [K]\{q\} = \{F_c\} + \{F_d\}. \tag{31}$$

3. Model reduction

When it comes to control system design and dynamic analysis, the full mathematical model given by Eq. (31) contains too many d.o.f. The GHM method models the viscoelastic effects through the introduction of extra dissipation co-ordinates, thus increasing the system order and making response calculations and controller design very computationally intensive. Therefore, it is indispensable that a model reduction be performed to bring the system back to its original size.

An iterative dynamic condensation [8] is performed.

Eq. (31) can be partitioned as

$$\begin{bmatrix} M_{mm} & M_{ms} \\ M_{sm} & M_{ss} \end{bmatrix} \begin{Bmatrix} \ddot{q}_m \\ \ddot{q}_s \end{Bmatrix} + \begin{bmatrix} D_{mm} & D_{ms} \\ D_{sm} & D_{ss} \end{bmatrix} \begin{Bmatrix} \dot{q}_m \\ \dot{q}_s \end{Bmatrix} + \begin{bmatrix} K_{mm} & K_{ms} \\ K_{sm} & K_{ss} \end{bmatrix} \begin{Bmatrix} q_m \\ q_s \end{Bmatrix} = \begin{Bmatrix} F_m \\ F_s \end{Bmatrix}. \tag{32}$$

Define dynamic condensation matrix $[\bar{R}]$ relating the master d.o.f.s with the slave d.o.f.s, after i iterations, the reduced order system equation is

$$[M_R^{(i)}]\{\ddot{q}_m\} + [D_R^{(i)}]\{\dot{q}_m\} + [K_R^{(i)}]\{q_m\} = \{F_R^{(i)}\}, \tag{33a}$$

where

$$\begin{aligned}
[M_R^{(i)}] &= [M_{mm}] + [\bar{R}^{(i)\mathrm{T}}][M_{sm}] + [M_{ms}][\bar{R}^{(i)}] + [\bar{R}^{(i)}]^{\mathrm{T}}[M_{ss}][\bar{R}^{(i)}], \\
[D_R^{(i)}] &= [D_{mm}] + [\bar{R}^{(i)}]^{\mathrm{T}}[D_{sm}] + [D_{ms}][\bar{R}^{(i)}] + [\bar{R}^{(i)}]^{\mathrm{T}}[D_{ss}][\bar{R}^{(i)}], \\
[K_R^{(i)}] &= [K_{mm}] + [\bar{R}^{(i)}]^{\mathrm{T}}[K_{sm}] + [K_{ms}][\bar{R}^{(i)}] + [\bar{R}^{(i)}]^{\mathrm{T}}[K_{ss}][\bar{R}^{(i)}], \\
\{F_R^{(i)}\} &= \{F_m\} + [\bar{R}^{(i)}]^{\mathrm{T}}\{F_s\}, \\
[\bar{R}^{(i+1)}] &= -[K_{ss}]^{-1}([M_{ss}][\bar{R}^{(i)}][M_R^{(i)}]^{-1}[K_R^{(i)}] - [K_{sm}]).
\end{aligned} \tag{33b–f}$$

Guyan condensation is taken as an initial iteration approximation [9], so $[\bar{R}^{(0)}] = -[K_{ss}]^{-1}[K_{sm}]$.

4. Output feedback optimal control

Based on the reduced model, an output feedback controller is designed. Eq. (33a) can be converted into the state-space form by introducing the state-space variable $\{x\}^{\mathrm{T}} = \{\{q_m\} \quad \{\dot{q}_m\}\}$.

$$\{\dot{x}\} = [A]\{x\} + [B]\{V_c\} + [B_d]\{F_{dR}\}, \tag{34}$$

$$\{V_s\} = [C]\{x\}, \tag{35}$$

where $\{F_{dR}\}$ is the reduced external disturbance force, $[A]$ is the system matrix; $[B]$ is the control matrix; $[B_d]$ is the disturbance matrix; and $[C]$ is the output matrix given by

$$\begin{aligned}
[A] &= \begin{bmatrix} [0] & [I] \\ -[M_R]^{-1}[K_R] & -[M_R]^{-1}[D_R] \end{bmatrix}, [B] = \begin{bmatrix} [0] \\ [M_R]^{-1}[B_o] \end{bmatrix}, \\
[B_d] &= \begin{bmatrix} [0] \\ [M_R]^{-1} \end{bmatrix}, [C] = [[\,C_o] \quad [0\,]].
\end{aligned} \tag{36a-d}$$

An optimal output feedback control scheme is adopted [10]. The control law is restricted to a linear time-invariant output feedback of the form

$$\{V_c\} = -[G_c]\{V_s\}, \tag{37}$$

where $[G_c]$ is the output feedback gain matrix to be determined. The cost function used to determine the gain matrix is given as

$$J = \int_0^\infty (\{x\}^{\mathrm{T}}[Q_c]\{x\} + \{V_c\}^{\mathrm{T}}[R_c]\{V_c\})\,\mathrm{d}t, \tag{38}$$

where $[Q_c]$ (positive semi-definite) and $[R_c]$ (positive definite) are weighting matrices to be selected by the designer. The optimal solution is found using the procedure in [11] that minimizes the expected value of performance index

$$J = \mathrm{tr}([P][X]), \tag{39}$$

where $[X] = E\{x(0)x^{\mathrm{T}}(0)\}$ and $[P]$ satisfies the Ricatti equation

$$[A_c]^{\mathrm{T}}[P] + [P][A_c] + [C]^{\mathrm{T}}[G_c]^{\mathrm{T}}[R_c][G_c][C] + [Q_c] = [0]. \tag{40}$$

By applying optimality conditions for above problem, the optimal control gain matrix $[G_c]$ can be obtained by solving the following coupled non-linear algebraic matrix equations simultaneously with Eq. (40).

$$[A_c][S] + [S][A_c]^{\mathrm{T}} + [X] = [0], \tag{41}$$

$$[G_c] = [R_c]^{-1}[B]^{\mathrm{T}}[P][S][C]^{\mathrm{T}}[[C][S][C]^{\mathrm{T}}]^{-1}. \tag{42}$$

Note that $[P]$, $[S]$ and $[G_c]$ are matrices to be determined from the above three equations. $[A_c]$ denotes the closed-loop system matrix

$$[A_c] = [A] - [B][G_c][C]. \tag{43}$$

Several numerical approaches are available for solving Eqs. (40)–(42). In this study, the effective iterative solution algorithm proposed by Moerder and Calise [12] is adopted.

5. Numerical example

To validate the reduced model, a clamped–free beam (Fig. 1b), with dimensions and parameters given in Table 1, is considered. The beam is disturbed at its free end. The transverse displacement response is measured there as well.

Table 1
System parameters

L	0.2616 m	h_b	0.002286 m	E_c	$6.49 \times 10^{10}\,\mathrm{N/m^2}$	G^∞	5×10^{-5} Pa
b	0.0127 m	ρ_c	$7600\,\mathrm{kg/m^3}$	E_s	$6.49 \times 10^{10}\,\mathrm{N/m^2}$	$\hat{\alpha}$	6.0
h_c	0.000762 m	ρ_v	$1250\,\mathrm{kg/m^3}$	E_b	$7.1 \times 10^{10}\,\mathrm{N/m^2}$	$\hat{\omega}$	10000 rad/s
h_v	0.00015 m	ρ_s	$7600\,\mathrm{kg/m^3}$	d_{31}	$-1.75 \times 10^{-10}\,\mathrm{m/V}$	$\hat{\zeta}$	4.0
h_s	0.000762 m	ρ_b	$2700\,\mathrm{kg/m^3}$	D'	$1.5 \times 10^{-8}\,\mathrm{F/m}$		

Table 2
Eigenvalues, modal frequencies and damping ratios of the first three vibration modes for full model (FM) and reduced model (RM)

		1st mode	2nd mode	3rd mode
FM	Eigenvalues:			
	Real (imaginary)	−2.553 (±226.03)	−14.851 (±1133.8)	−11.944 (±3018.6)
	Modal freq. (Hz)	35.97	180.45	480.43
	Damping ratios (%)	1.129	1.309	0.396
RM	Eigenvalues:			
	Real (imaginary)	−2.536 (±226.18)	−14.832 (±1133.7)	−11.903 (±3018.6)
	Modal freq. (Hz)	35.99	180.43	480.43
	Damping ratios (%)	1.121	1.308	0.394

Table 3
Relative errors of modal frequencies and damping ratios of reduced model

	Relative error of modal frequency (%)	Relative error of damping ratio (%)
1st mode	0.056	0.709
2nd mode	0.011	0.764
3rd mode	0	0.505

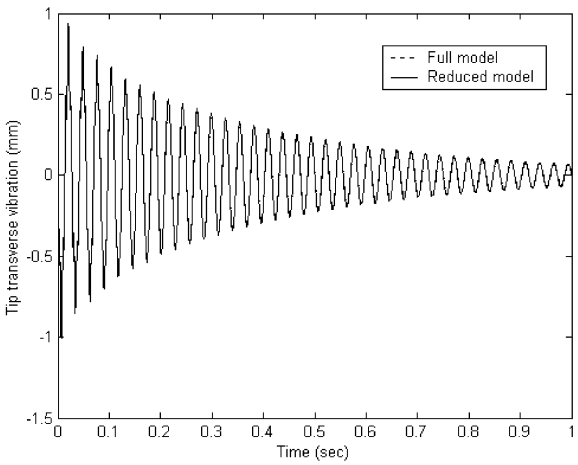

Fig. 4. Tip transverse vibration under impulse disturbance.

The whole structure is divided into 11 elements (the number of elements used in the interspaces, each ACLD element, and rest of the beam at the free end are one, three and three respectively). Following the procedures described in Section 3, a model reduction is performed. Constrained by ACLD requirements, all the dissipation co-ordinates are selected to be slave d.o.f.s. All others are master d.o.f.s. Table 2 shows eigenvalues, modal frequencies and modal damping of the first three vibration modes for the full model (FM) and reduced model (RM). Table 3 presents the relative

errors of the modal frequencies and modal damping of the RM. Fig. 4 is the transverse vibration response at the free tip under an impulse disturbance. All these results indicate that the influence of the truncated modes is negligible. Consequently, the reduced models are used for control system design and analysis.

6. Comparisons among various configurations

To establish the hybrid damping systems, optimal output feedback approach is used, as described in Section 4. The weighting matrices are $[Q_c] = q[\bar{Q}_c]$ and $[R_c] = [I]$, where q represents the weighting corresponding to the transverse vibration states only. q is the only design parameter which is adjusted to obtain maximum damping ratio, and at the same time without making the

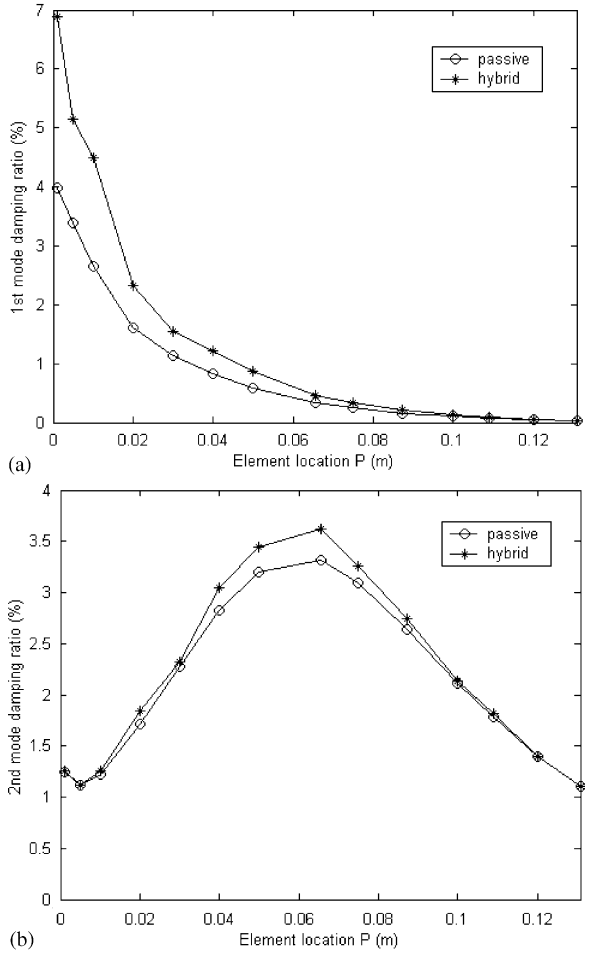

Fig. 5. (a) Effect of location P on the 1st mode damping ratios—Case I. (b) Effect of location P on the 2nd mode damping ratios—Case I.

close-loop system unstable. Besides, the voltage applied to the actuator could not exceed the breakdown voltage of the piezoelectric material.

To investigate the effects of different treatment configurations, subjected to total treatment length (0.1308 m) and height ($h_c + h_v + h_s = 1.674$ mm) constraints, on the damping characteristics of the beam, two cases are considered—(I) one ACLD element (Fig. 1a) and (II) two ACLD elements (Fig. 1b). In Case I, the passive and hybrid damping ratios of the first two modes are plotted as function of element location P (Fig. 5). In Case II, the passive and hybrid damping ratios of the first two modes are plotted as function of element spacing S for various location P (Figs. 6–9).

In Case I, it can be observed from Fig. 5a that for the first mode, both the passive and hybrid damping decrease with increase in distance between the fixed end and the left end of the element. For the second mode, as shown in Fig. 5b, the damping ratio initially decreases with the departure of the element, and increases with further departure and then decreases again. In both modes, it

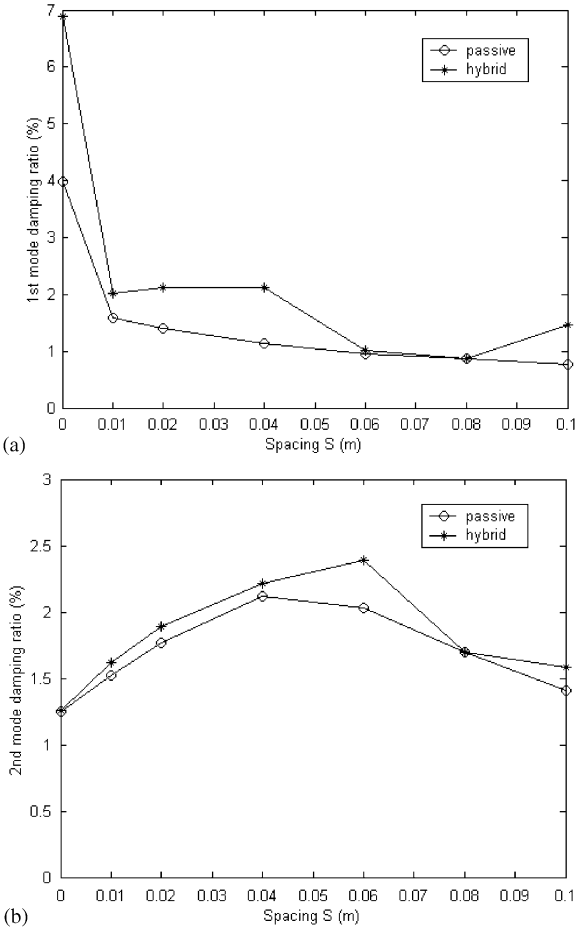

Fig. 6. (a) First mode damping ratios as function of spacing S—Case II, $P = 0.001$ m. (b) Second mode damping ratios as function of spacing S—Case II, $P = 0.001$ m.

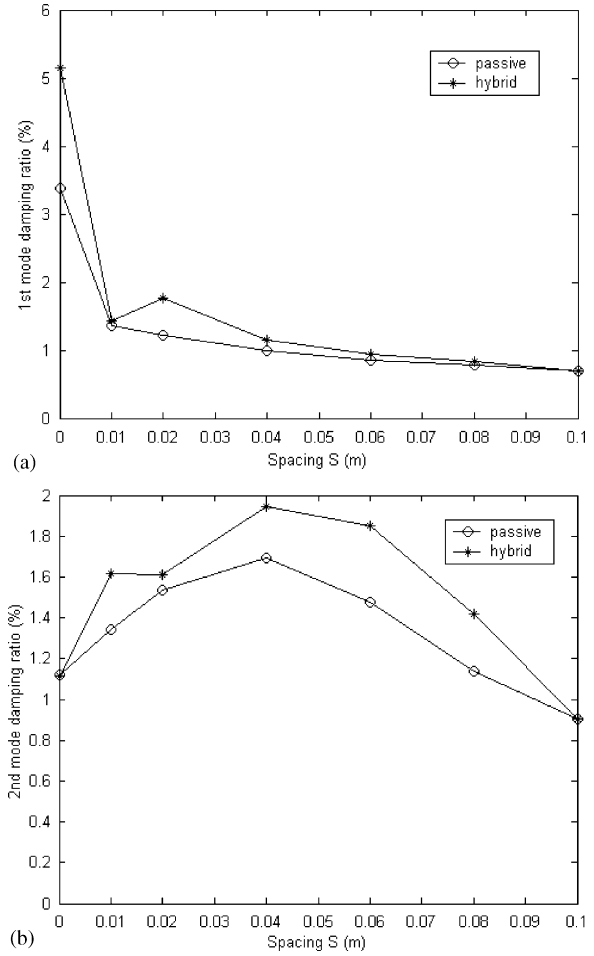

Fig. 7. (a) First mode damping ratios as function of spacing S—Case II, $P = 0.005$ m. (b) Second mode damping ratios as function of spacing S—Case II, $P = 0.005$ m.

can be seen that the hybrid damping is more effective for a configuration with higher passive damping. Figs. 6–9 show the effects of different combinations of element location P and spacing S on the damping ratios of the first two modes for Case II.

Results in Figs. 5–9 are analyzed and comparisons are given in Table 4. It can be observed from Table 4 that placing a single ACLD element at about $P = 0.003$ m, the hybrid damping ratio of the first and second modes are 6% and 1.2%, respectively. Moving the element to about $P = 0.048$ m can increase the hybrid damping ratio of the second mode to about 3.4%, but at the same time decreases the hybrid damping ratio of the first mode to 1%. Table 4 also reveals that a two-element configuration, with an appropriate combination of P and S, can yield a higher second mode damping as compared to a single-element configuration. Table 5 shows that a maximum improvement of 31% on the second mode damping can be obtained with $P = 0.001$ m and $S = 0.004$ m, when the first mode damping ratio is 5%.

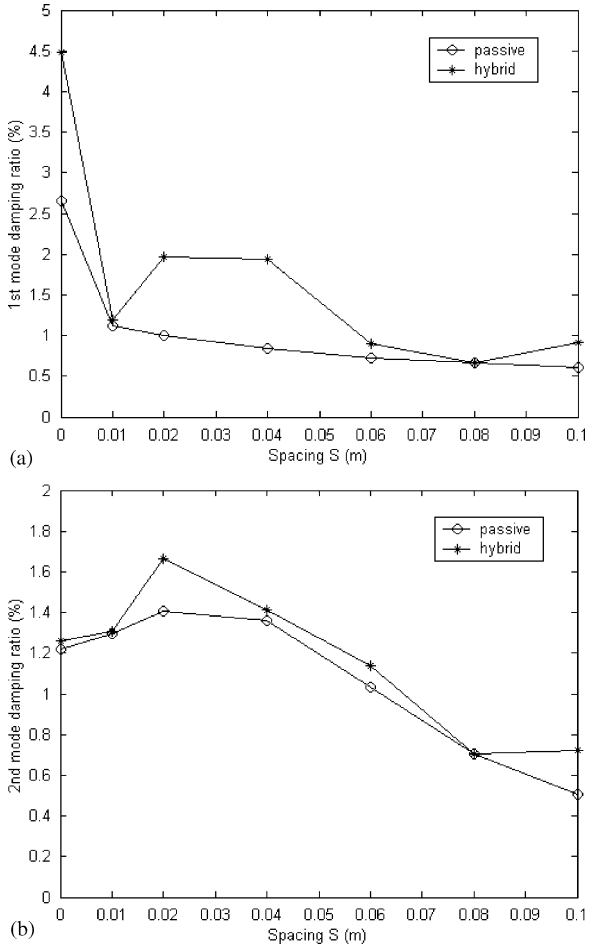

Fig. 8. (a) First mode damping ratios as function of spacing S—Case II, $P = 0.01$ m. (b) Second mode damping ratios as function of spacing S—Case II, $P = 0.01$ m.

7. Conclusions

In the present study, a clamped–free beam with partial active constrained layer damping (ACLD) treatment is modelled by using the finite element method. The Golla–Hughes–McTavish (GHM) method is employed to account for the frequency-dependent characteristic of the viscoelastic material (VEM). As the resultant finite element model contains too many d.o.f.s. due to the introduction of dissipative coordinates, a model reduction is performed to bring the system back to its original size. Finally, optimal output feedback gains are designed based on the reduced models. Numerical simulations are performed to study the effect of different ACLD treatment configurations, with various element numbers, spacing and locations, on the damping performance of a flexible beam. Results are presented for the damping ratios of the first two vibration modes for two different cases (one element in Case I and two elements in Case II). It is found that to enhance the second mode damping, without deteriorating the first mode damping,

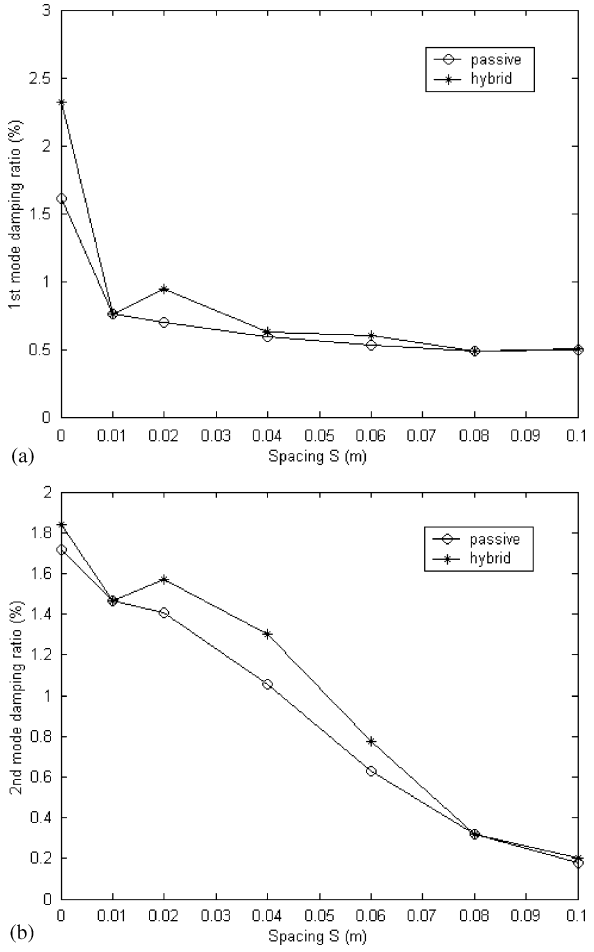

Fig. 9. (a) First mode damping ratios as function of spacing S—Case II, $P = 0.02$ m. (b) Second mode damping ratios as function of spacing S—Case II, $P = 0.02$ m.

Table 4
Comparison of 2nd mode damping ratios among various configurations in Cases I and II for given values of 1st mode damping

1st mode damping ratio (%)	Case I		Case II		
	P (m)	2nd mode damping ratio (%)	P (m)	S (m)	2nd mode damping ratio (%)
6	0.003	1.2	0.001	0.002	1.30
5	0.007	1.1	0.001	0.004	1.45
4	0.013	1.4	0.001	0.006	1.50
3	0.018	1.6	0.001	0.007	1.55
2	0.025	2.1	0.001	0.042	2.20
1	0.048	3.4	0.001	0.060	2.45

Table 5
Differences of 2nd mode damping ratios between Cases I and II in Table 4.

1st mode damping ratio (%)	1	2	3	4	5	6
Difference of 2nd mode damping ratios between Cases I and II (%)	−27.94	4.76	−3.13	7.14	31.82	8.33

splitting a single ACLD element into two and placing them at appropriate positions of the beam could be a possible solution.

Acknowledgements

The authors would like to thank the Research Committee of The Hong Kong Polytechnic University for funding the project in the form of research studentship. They also wish to thank the reviewers for their useful comments.

Appendix. Nomenclature

$[A]$	system matrix
$[A_c]$	close-loop system matrix
$[B]$	control matrix
$[B_d]$	disturbance matrix
b	width of beam
$[C]$	output matrix
C_a	capacitance of the sensor layer
D	electrical displacement
D'	absolute permittivity of sensor layer
d_{31}	piezoelectric constant
$[D]$	damping matrix
$E_{c,s,b}$	Young's modulus of constraining layer, sensor layer and base beam respectively
E	electrical field
$\{f_c\}_e$	force of constraining layer
$\{f_d\}_e$	force of external disturbances
G_c	control gain
G^∞	equilibrium value of shear modulus
G_v	shear modulus of VEM in time domain
$h_{c,v,s,b}$	thickness of constraining layer, VEM layer, sensor layer and base beam, respectively
$I_{c,s,b}$	moment of inertia of constraining layer, sensor layer and base beam, respectively
$[K]$	stiffness matrix
L_e	length of treated beam elements
L	length of base beam
$[M]$	mass matrix

$N_{w,\theta,u_c,u_v,u_s,u_b,\gamma}$	shape functions of the transverse displacement, rotational angle, the axial displacement of constraining layer, the axial displacement of VEM layer, the axial displacement of sensor layer, the axial displacement of base beam and the shear strain of VEM layer, respectively
$\{q\}$	displacement vector
$[\bar{R}]$	dynamic condensation matrix
S_{11}^{E}	elastic compliance constant
$s\tilde{G}(s)$	complex modulus of VEM layer
$\{U\}_e$	local nodal displacement vector
$u_{c,s,b}$	axial displacement of constraining layer, sensor layer and the base beam
$V_{c,s}(t)$	control and sensed voltages of the constraining layer and senor layer, respectively
w	transverse displacement
$\hat{Z}(s)$	dissipation co-ordination
$\hat{\alpha}, \hat{\omega}, \hat{\zeta}$	positive constants of GHM model
γ	shear strain of VEM layer
ε	mechanical strain in the axial direction
ε_{33}^{τ}	dielectric constant
θ	rotational angle
$\rho_{c,v,s,b}$	density of constraining layer, VEM layer, sensor layer and base beam respectively
σ	mechanical stress in the axial direction

Superscript

$'$	partial differentiation with respect to x

Subscripts

b	base beam
c	constraining layer
i,j	elemental node i,j
m	master d.o.f.s
s	slave d.o.f.s
R	reduced order system
u	axial displacement
v	viscoelastic layer
w	transverse displacement
γ	shear strain of VEM layer

References

[1] S.C. Huang, D.J. Inman, E.M. Austin, Some design considerations for active and passive constrained layer damping treatments, Smart Materials and Structures 5 (1996) 301–313.

[2] M.A. Trindade, A. Bedjeddou, R. Ohayon, Modeling of frequency-dependent viscoelastic materials for active-passive vibration damping, American Society of Mechanical Engineers, Journal of Vibration and Acoustics 122 (2000) 169–174.
[3] A. Baz, J. Ro, Optimum design and control of active constrained layer damping, American Society of Mechanical Engineers, Journal of Mechanical Design 117B (1995) 135–144.
[4] W.H. Liao, K.W. Wang, On the analysis of viscoelastic materials for active constrained layer damping treatments, Journal of Sound and Vibration 207 (1997) 319–334.
[5] IEEE Standard on Piezoelectricity, 1987, ANSI-IEEE Std 176-1987.
[6] D.J. McTavish, P.C. Hughes, Modeling of linear viscoelastic space structures, American Society of Mechanical Engineers, Journal of Vibration and Acoustics 115 (1993) 103–110.
[7] D.F. Golla, P.C. Hughes, Dynamics of viscoelastic structures—a time-domain finite element formulation, American Society of Mechanical Engineers, Journal of Applied Mechanics 52 (1985) 897–906.
[8] Z.Q. Qu, A multi-step method for matrix condensation of finite element models, Journal of Sound and Vibration 214 (1998) 965–971.
[9] Y.M. Shi, Z.F. Li, H.X. Hua, Z.F. Fu, T.X. Liu, The modeling and vibration control of beams with active constrained layer damping, Journal of Sound and Vibration 245 (2001) 785–800.
[10] Y.-H. Lim, S.V. Gopinathan, V.V. Varadan, V.F. Varadan, Finite element simulation of smart structures using an optimal output feedback controller for vibration and noise control, Smart Materials and Structures 8 (1999) 324–337.
[11] W.S. Levine, M. Athans, On the determination of the optimal constant output feedback gains for linear multivariable systems, IEEE Transactions on Automatic Control 15 (1970) 44–48.
[12] D.D. Moerder, A.J. Calise, Convergence of a numerical algorithm for calculating optimal output feedback gain, IEEE Transactions on Automatic Control 30 (1985) 900–903.